Energy and Environment Research; Vol. 13, No. 1; 2023
ISSN 1927-0569 E-ISSN 1927-0577
Published by Canadian Center of Science and Education

CFD Simulation of Temperature and Air Flow in a Natural Convection Solar Tunnel Dryer with a Bare Flat-Plate Chimney

Maona Mukanema[1] & Isaac N. Simate[2]

[1] Department of Mechanical Engineering, School of Engineering, University of Zambia, Lusaka, Zambia

[2] Department of Agricultural Engineering, School of Engineering, University of Zambia, Lusaka, Zambia

Correspondence: Maona Mukanema, Department of Mechanical Engineering, School of Engineering, University of Zambia, Lusaka, Zambia. E-mail: maonamukanema@gmail.com

Received: January 30, 2023 Accepted: February 26, 2023 Online Published: February 27, 2023

doi:10.5539/eer.v13n1p1 URL: https://doi.org/10.5539/eer.v13n1p1

Abstract

Computational Fluid Dynamics simulation of a natural convection solar tunnel dryer with a bare flat-plate chimney is presented. The chimney's function is to create airflow in the dryer through the buoyancy effect by re-heating the air coming from the drying unit and is therefore a major factor in the drying rate. CFD simulation was therefore employed to study the temperature and airflow in the dryer and determine the areas that could be improved upon. The design of the solar tunnel dryer geometry used in this simulation was done in SOLIDWORKS 2016 whereas the simulation of temperature distribution of airflow inside the dryer was performed using SOLIDWORKS 2016 flow simulation program in a steady-state regime. The boundary conditions were set using the obtained experimental data. The simulation results showed that the chimney losses heat, that there is air recirculation in the collector, that the airflow experiences some pressure loss as it moves from the drying chamber to the chimney, and that there is some reduction of the velocity in some parts of the dryer. The simulated and experimental collector efficiencies were found to be 33.09 and 37.63%, respectively, giving a mean relative deviation of collector temperature of 5.1%. To improve the performance of the dryer, insulating and glazing of the chimney is suggested as well as using a curved joint between the chimney and the drying chamber.

Keywords: CFD simulation, temperature and airflow, natural convection, solar tunnel dryer, chimney

1. Introduction

Natural convection solar dryers do not use fans and therefore have advantages over forced convection solar dryers in terms of operations in rural or remote settings where there is no electricity grid and where installed solar PV panels are prone to theft (Simate & Cherotich, 2017). In both natural and forced convection solar dryers, heated air is key to the performance of the dryer as it supplies all/some of the heat to the food to evaporate the moisture, as well as take away the evaporated moisture (Bala & Wood, 1994). A study of the airflow behaviour in the dryer can help develop better performance solar dryers (Simate, 2020). The drying rate is a strong function of airflow and it is of great importance to know the areas of adequate air velocities for proper drying (Xia & Sun, 2002). Mathioulakis et al. (1998) showed, using CFD that the degree of fruit dryness depended on its position within the dryer. Kaushal and Sharma (2012) determined the pressure profiles and air velocities using CFD and showed that the main cause of the variations in drying rates and moisture contents was the lack of spatial homogeneity of air velocities within the dryer. For a natural convection solar dryer, Al-Neama & Farkas (2016) showed that the velocity of air in the chimney was a function of temperature change across the chimney. Vintilă et al. (2014) used CFD in natural convection solar dryers to simulate the temperature distribution and velocity field in the collector and drying chamber. Omolola et al. (2015) conducted a CFD analysis of a solar dryer using SolidWorks Flow Simulation. They investigated the effect of airflow distribution, flow velocity, and pressure field on transient moisture within the dryer. Some of the simulation parameters such as air temperature were accurately predicted resulting in small deviations of about 0.02%. Their simulation of the drying process for the green bell pepper was conducted using the standard turbulence model under steady-state conditions. Zoukit et al. (2019) used SolidWorks and presented a numerical simulation of a hybrid solar-gas dryer operated under forced convection with an air mass flow rate of 0.025kg/s. Jhersson et al. (2018) also used SolidWorks to simulate velocity and temperature in a food dyer in order to define the contours with the aim of evaluating the operating conditions of the chamber and found that the design having outlets on both sides with horizontally inclined trays gave the best performance. According to Misha et al. (2013), CFD can be a valuable tool for engineering design and analysis of complex fluid flow situations, addressing heat and mass transfer phenomena, aiding in the better design of tray dryers, and production of high-quality dried products. One type of natural convection solar dryer, the natural convection solar tunnel dryer, has shown great potential in drying fruits such as mango and banana. This type of dryer has a distinct collector unit that heats the air, a drying unit where the product is located and, a bare flat-plate chimney that creates buoyancy by re-heating the air coming from the drying unit. However, one drawback with this dryer is the temperature of the air in the chimney being lower than that of air coming from the drying unit, implying that the chimney losses heat to the environment, consequently reducing the air flow rate and, ultimately, the drying rate (Cherotich & Simate, 2016). Since the airflow through a natural convection solar dryer is initiated by the buoyancy-induced pressure head that is created above the atmospheric pressure, any changes in the chimney air temperature affect the air flow and temperature in the collector and drying chamber. It was therefore the objective of this study to use CFD to model the temperatures and airflow in the dryer and identify factors contributing to air temperature and flow and, areas that could be improved upon.

2. Materials and Methods

2.1 Description of the Dryer and its Components

The natural convection solar tunnel dryer designed by Cherotich, (2016) and presented by Cherotich and Simate (2016) was modeled and simulated using SolidWorks Flow simulation developed by Dassault systems. Figure 1 shows the modeled natural convection solar tunnel dryer. The dryer consists of a collector unit, a drying unit, and a bare flat-plate chimney unit. The solar collector unit is a flat-plate type. The absorber plate is made from a 0.3 mm thick flat Galvanized Iron (GI) sheet and its top side is painted matt black (absorptivity = 0.95, emissivity = 0.8). The collector is covered with a transparent 200 μm polythene sheet (transmissivity = 0.857) which allowed the solar radiation to heat the absorber, consequently heating the ambient air entering the collector and moving to the drying unit. The drying unit, also covered with the same polythene sheet, and the collector unit, were made in one subassembly and from the same materials, and are configured in series. The drying unit contains a removable wire mesh tray to hold the product during drying. Then the drying unit is linked to a chimney. The chimney is a bare flat-plate type collector also constructed from a 0.3 mm thick flat GI sheet and painted matt black to absorb most of the incident solar radiation falling on it so as to reheat the air exiting the drying unit.

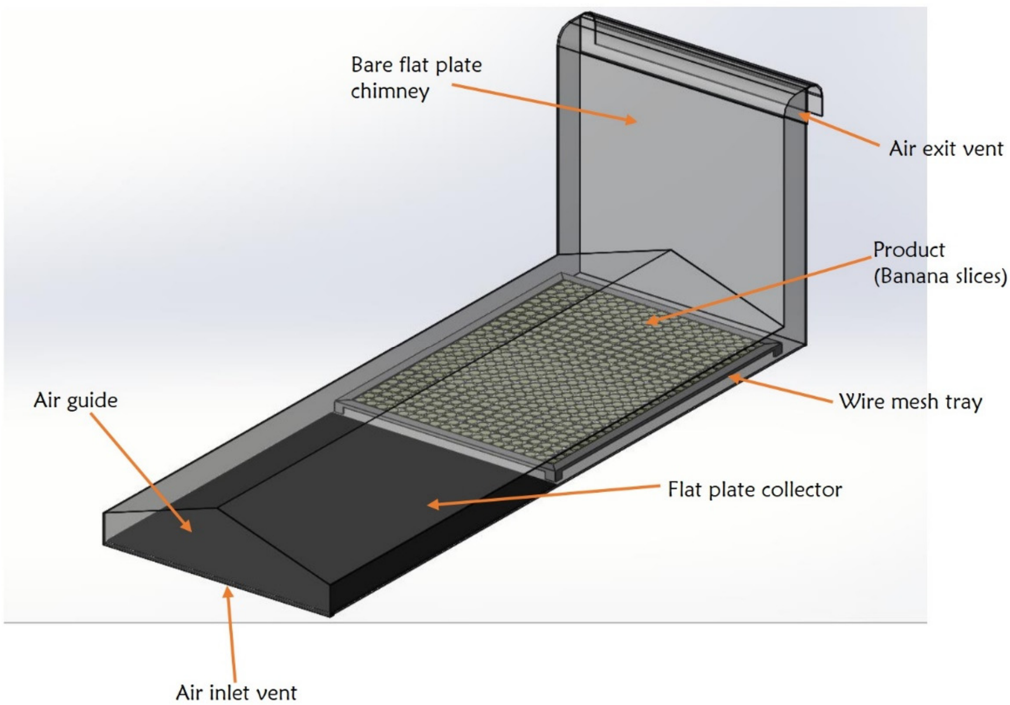

Figure 1. Modelled natural convection solar tunnel dryer

2.2 Experimentation

The experiments were conducted on the solar tunnel dryer at the field station of the Department of Agricultural Engineering, University Zambia, Lusaka Zambia (Latitude 15.3°S; Longitude 28.3°E). Drying experiments using fresh banana slices were conducted in April 2022. The simulation was performed with banana slices in the drying unit. The results of the load condition were used to illustrate the velocity and temperature contours. Simulating the inceptive conditions of the experiment was done to validate the result.

2.3 Simulation Procedure

SOLIDWORKS 2016 was utilized to produce a 3 Dimensional (3D) geometry of the solar tunnel dryer. CPU Type: Intel(R) Core(TM) i5-5300U CPU @ 2.30GHz, CPU Speed: 2295 MHz, RAM: 3970 MB, Flow Simulation 2016 SP0.0. Build: 3259 helps provide valuable data to pinpoint the system's low temperature points and this knowledge will be helpful for optimizing and advancing solar tunnel dryer design. The boundary conditions for pressure (environmental pressure) and mass flow rate were set at the inlet and outlet of the geometric model. To perform the computation, the k-ε turbulence model was chosen because it yielded precise and acceptable results. After the creation of a 3D geometric model of the solar tunnel dryer shown in Figure 2, the configuration of the Flow simulation project was done.

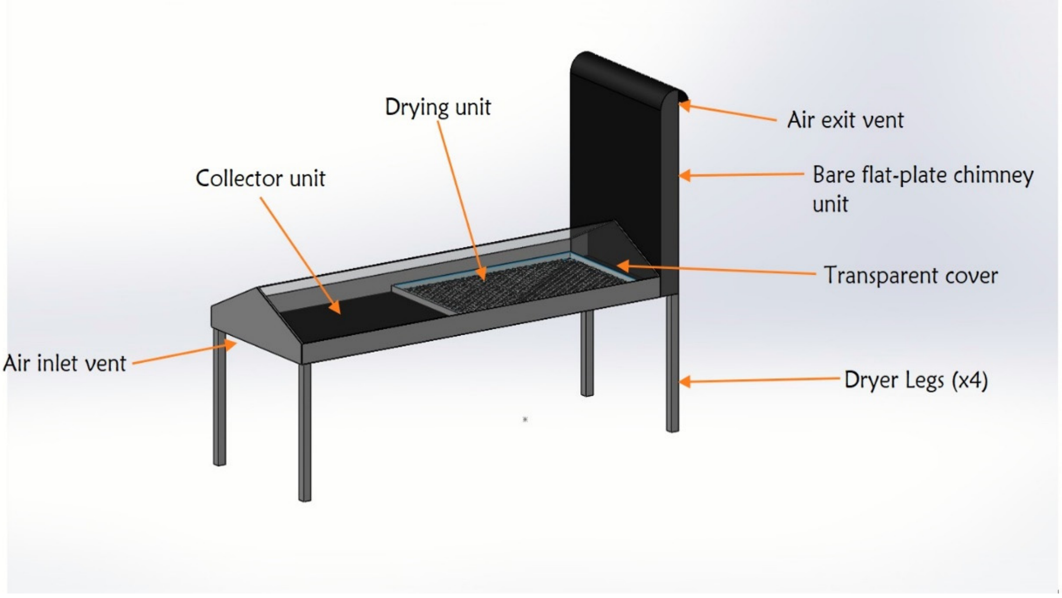

Figure 2. Solar tunnel dryer geometric model

2.3.1 Flow Simulation Project Configuration

For the internal flow analysis, specific information about the decline in pressure as a function of the flow of mass is provided. The goal of the project is to produce a simulation for fluid dynamics using computational fluid dynamics (CFD) where the following are defined: Unit system, Analysis type (internal analysis and excluding the cavities without conditions of flow), Fluid (Air, flow type: Laminar) and Initial conditions. This study employed the following simulation procedure.

2.4 Setting up a 3D Flow Condition

2.4.1 Computational Domain

The area around the 3D model, which defines the flow simulation in the restricted area, is known as the Computational Domain. This defines the boundary under which the flow simulation will take place. It is within the Computational Domain where flow and heat transfer calculations are carried out. The Computational Domain is a rectangular prism for the 3D analyses. The Computational Domain boundaries are parallel to the global coordinate system planes. The icon Computational Domain is used to modify the dimensions of the volume that it is being analysed and it allows visualizing the limits of the Computational Domain (SOLIDWORKS Corporation, 2010). Table 1 shows the coordinates of the Computational Domain size, and Figure 3 shows the visualization of the Computational Domain.

Table 1. Computational Domain size

Axis	size
X min	0.345 m
X max	1.091 m
Y min	1.037 m
Y max	1.789 m
Z min	0.442 m
Z max	2.546 m

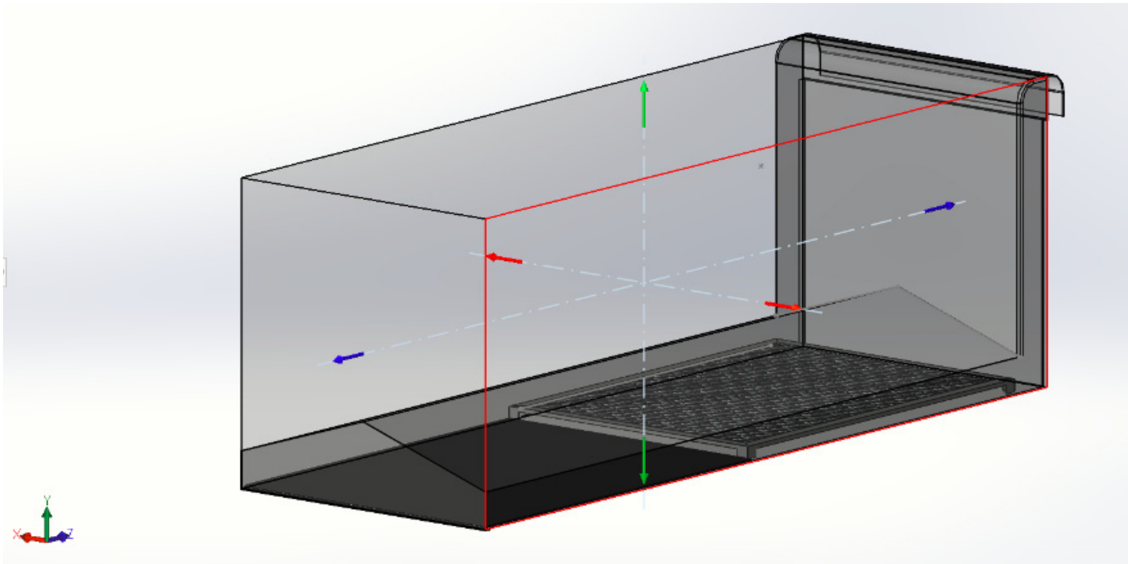

Figure 3. Visualization of Computational Domain

2.4.2 Material Properties

The properties of materials used in the simulation study are shown in Table 2.

Table 2. Material properties

Parameter	Value	Units	Source
Banana dimension (D × h)	30 × 3	mm	In this study
Initial moisture content - Ripe banana	73.8	%w.b.	In this study
Initial Equivalent porosity - Ripe banana	0.83	-	(Ni, 1997)
Thermal conductivity - Ripe banana	0.97	W/m K	(Udomdejwatana, 1994)
Density - Ripe banana	870	Kg/m^3	
Specific heat capacity (Cp) - Ripe banana	3,430	J/kg K	
Ambient pressure	10,1325	Pa	In this study
Polyethylene Cover			(Roman, Lopez, Garcia, Pilatosky, & Ituna, 2019)
-Density	915	Kg/m^3	
-Thermal conductivity	0.33	W/m K	
-Emissivity	0.9	-	
-Specific heat capacity (Cp)	1,900	J/kg K	
Single-layer polyethylene sheet			(Michael, 2014)
-Transmittance	85.7	%	
Galvanized iron sheet			(Kumar, Sreenivaslu, P S Raghavendra, Kumar, & Pattanaik, 2019)
-Density	7,870	Kg/m^3	
-Thermal Diffusivity	84.18x10^6	m^3/s	
-Specific Heat (Cp)	896	J/kg K	
-Thermal Conductivity (k)	204.2	W/m K	

2.4.3 Applying Boundary Conditions

In this study, the boundary conditions in regard to pressure and mass flow, and the dryer's surfaces (top cover, floor, and sides) were considered to be no-slip walls for the purpose of fluid flow analysis. These surfaces also had adiabatic considerations. The top cover had a boundary condition to simulate incident sunlight upon the dryer. The collector was modeled with radiation and a characteristic of rough galvanized iron. The plastic cover making up the dryer's roof was modeled to have a transmissivity of 0.86, the average light transmissivity for polyethylene plastic film (Sangpradit, 2014). The model geometry was characterized by a laminar flow regime.

2.4.4 Porous Medium

The porous medium icon allows the selection of components to be treated as such, using information from the engineering database (SOLIDWORKS Corporation, 2010). The banana was considered as porous media in the solar tunnel dryer. Figure 4 shows the arrangement of banana slices on the mesh. The porous media is modelled by the addition of a momentum source term to the standard fluid flow equations such as conservation of energy, momentum, and moisture transport equation. For this simulation study, the banana porosity was assumed to be constant.

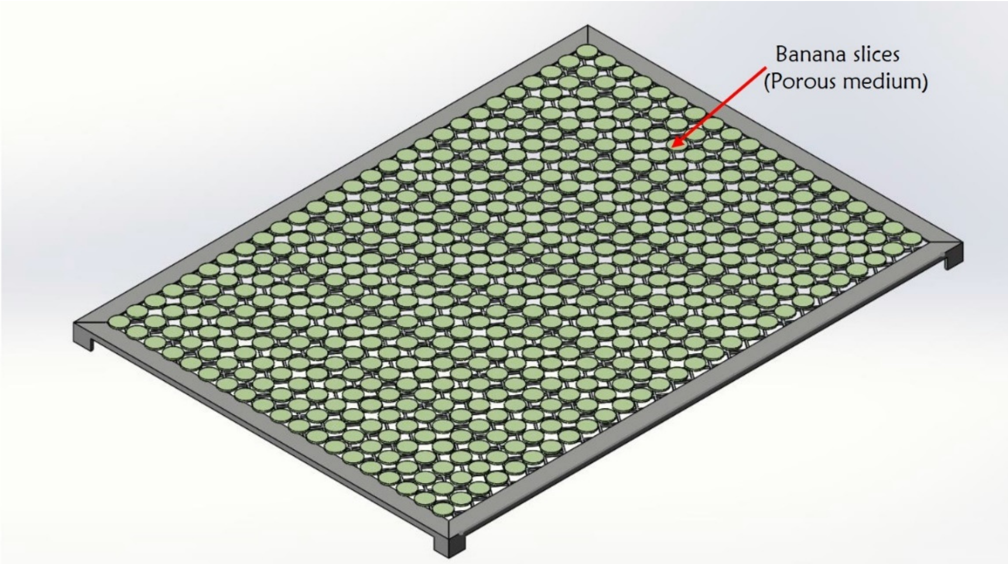

Figure 4. Arrangement of the bananas on the mesh

2.4.5 Initializing the Mesh

When the model is meshed, computational cells are created within the model and Computational Domain. Therefore, subdividing a model into a continuous set of nodes and elements, i.e., meshing a model, is a necessary prerequisite in the solution process. Fortunately, within SOLIDWORKS, simulation meshing occurs automatically. The operation can also be used to define the motion of the system and the analyses of simulation. The discretization process produced Total cell count, Fluid cells, Solid cells, and Partial cells equal to 760769, 324003, 262828, and 173938 respectively, these were used in the simulation analysis. Figure 5 shows the generated mesh of the solar dryer model.

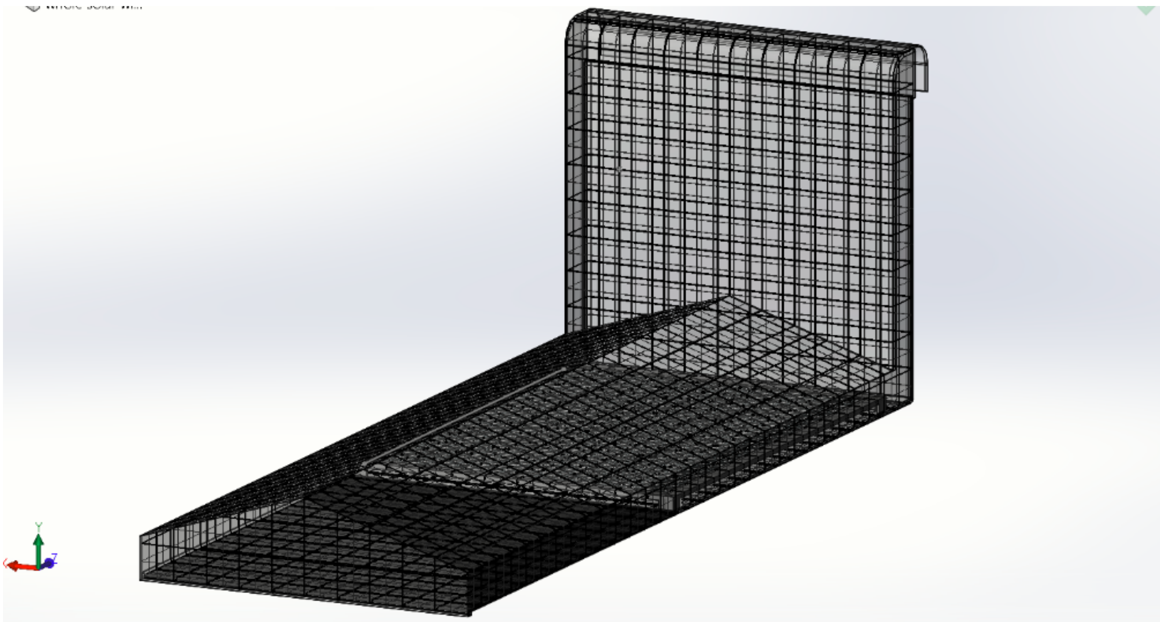

Figure 5. Generated Mesh

2.5 Running the Calculation

The simulation was run, and the process of convergence which is iterative, began. Due to the restrictions imposed on each parameter by the discretization of the flow field, no parameter can acquire a perfectly stable value, but will instead oscillate near it from iteration to iteration.

2.6 Visualization of the Temperature Flow Field

Once the calculation is done, the results of the saved computations can be modified and seen in a variety of ways right in the graphics area. The following features were used to view the results: cut plots, surface plots, flow trajectories, point parameters, surface parameters, goals, reports, and result animations.

2.7 Mean Relative Deviation

The model-predicted results were validated with experimental results using statistical analysis. The prediction ability of the model was tested by a statistical measure known as mean relative deviation (MRD) described by Equation (1). The mean relative deviation gives an idea of the mean departure of the measured data from the simulated data. The acceptable mean relative deviation should not exceed 10%.

$$MRD = \frac{1}{m}\sum_{i=1}^{m}\frac{|Simulated(i) - Measured\ (i)|}{Simulated(i)} \quad (1)$$

2.8 Calculation of the Collector Efficiency

Collector efficiency (η_c) is a measure of the efficacy of transfer of the solar insolation incident upon the collector to the air flowing through the collector (Tiris, Tiris, & Dincer, 1995). It was used to evaluate the performance of a flat-plate collector and is described by Equation (2).

$$\eta_c = \frac{\dot{m}C_p(T_c - T_{am})}{I_s A_c} \quad (2)$$

Where A_c = collector area, m^2

I_s = mean solar insolation, W/m^2

T_c = mean collector air temperature, ^oC

T_{am} = mean ambient air temperature, ^oC

C_p = specific heat capacity of air, J/kg ^oC

$\dot{m}$ = air mass flow rate, kg/s

3. Results and Discussion

3.1 Simulation of the Natural Convection Solar Tunnel Dryer

The temperature distribution inside the solar tunnel dryer was determined through simulation. The simulations were carried out while taking into account the porous nature of bananas. This simulation was seeking to define the working fluid's (air) temperature and velocity contours inside the tunnel dryer.

3.1.1 Temperature

The fluid temperature flow trajectories inside the solar dryer at 09:00, 12:00 and 15:00 hours are depicted in Figure 6. It is evident from Figure 6 that air at the flat plate collector entry is at ambient temperature and increases towards the top of the collector as it enters the drying unit. The temperature of air adjacent to the collector plate increased as visualized in the figure. The tunnel temperature remains higher than the ambient temperature. It can also be noted that the temperature at various locations of the dryer varies with time. The solar dryer temperature is increasing steadily with the increase in solar insolation. The temperature of the air at the collector outlet ranged between 49.03 and 66.82℃. The heated air moved from the solar collector to the drying unit. The air was observed to have increased in temperature at the drying unit due to the mixed mode design of the dryer. The temperatures inside the drying unit ranged between 55.12 and 73.97 ℃. The difference in temperature between the middle and the edge of the removable wire mesh tray located in the drying unit was deemed insignificant, and it can be assumed that the current design was successful in achieving a suitable uniform air temperature. The results of the simulation revealed that the average drying air temperature at the collector and drying unit were 56.71 and 62.9 ℃, respectively, but the maximum hourly simulated maximum temperatures in the collector and drying unit were 66.83 and 73.9℃, respectively. The lowest temperatures were observed in the chimney and ranged from 38.78 to 59.9℃ with an average of 51.38℃. These results are comparable to the simulation of a hybrid solar-gas dryer in solar mode done by Zoukit et al. (2019) who obtained temperature and relative humidity inside the drying chamber in the range of 50 to 60℃ and 10 to 6.2%, respectively.

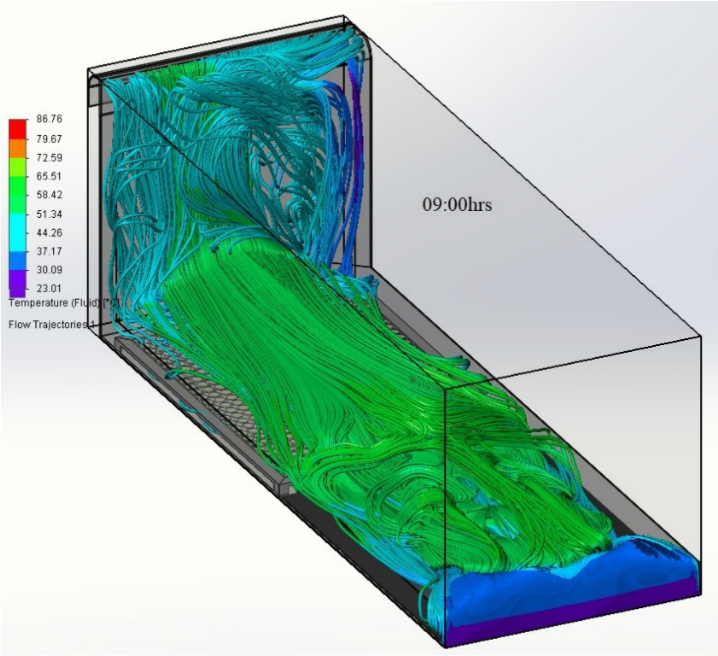
86.76
79.67
72.59
65.51
58.42
51.34
44.26
37.17
30.09
23.01
Temperature (Fluid) [°C]
Flow Trajectories 1
09:00hrs

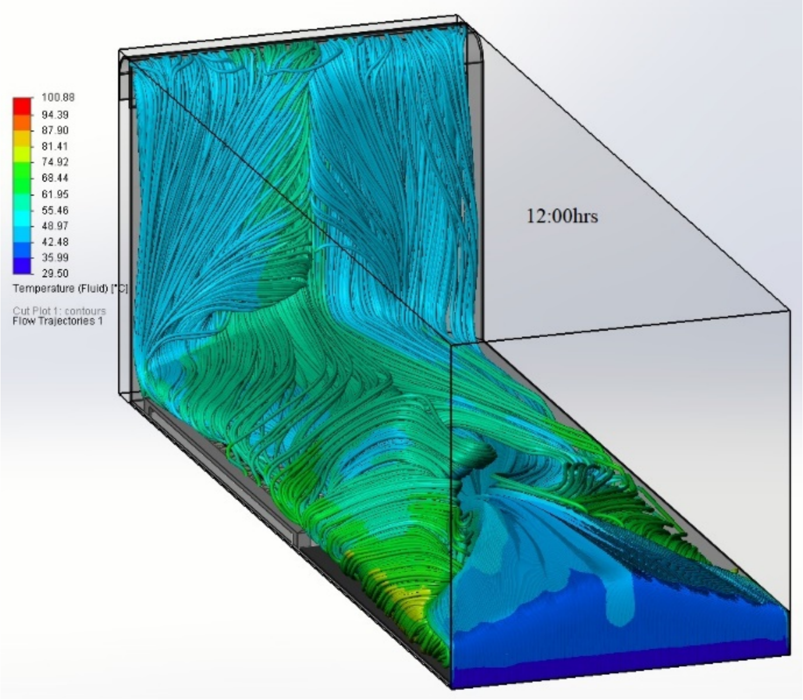
100.88
94.39
87.90
81.41
74.92
68.44
61.95
55.46
48.97
42.48
35.99
29.50
Temperature (Fluid) [°C]
Cut Plot 1: contours
Flow Trajectories 1
12:00hrs

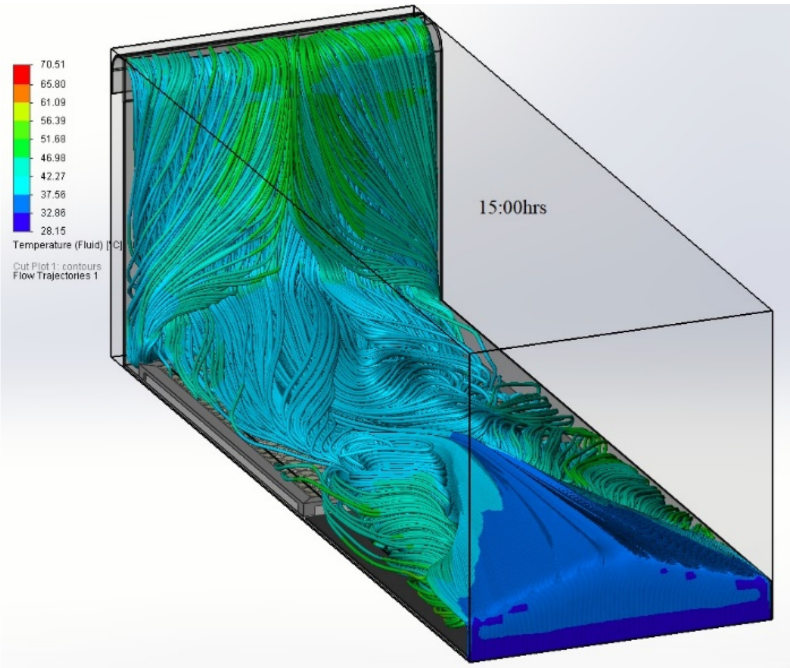

Figure 6. Temperature flow trajectories

Figure 7 shows temperature cut plot at 14:00 hours. From the visualization of air temperature distribution across the collector and drying unit, it can be noticed that the maximum heat gain is at the collector and this is a similar trend observed from the experiment. The air temperature near the wall is slightly lower compared to that at the centre of the drying chamber. It is due to the shortest path followed by air to exit the dryer (which can also be observed from the flow trajectories in Figure 6). It was observed that although the chimney was receiving solar insolation through its absorber (the side facing the drying chamber), the air in the chimney did not seem to have benefited from this heating as its temperature remained at the same level as that it came with from the drying chamber. This is an indication that there was some loss of heat from the air passing through the chimney. One way of reducing the heat loss from the chimney is to insulate the back and sides of the chimney and add glazing on the front side.

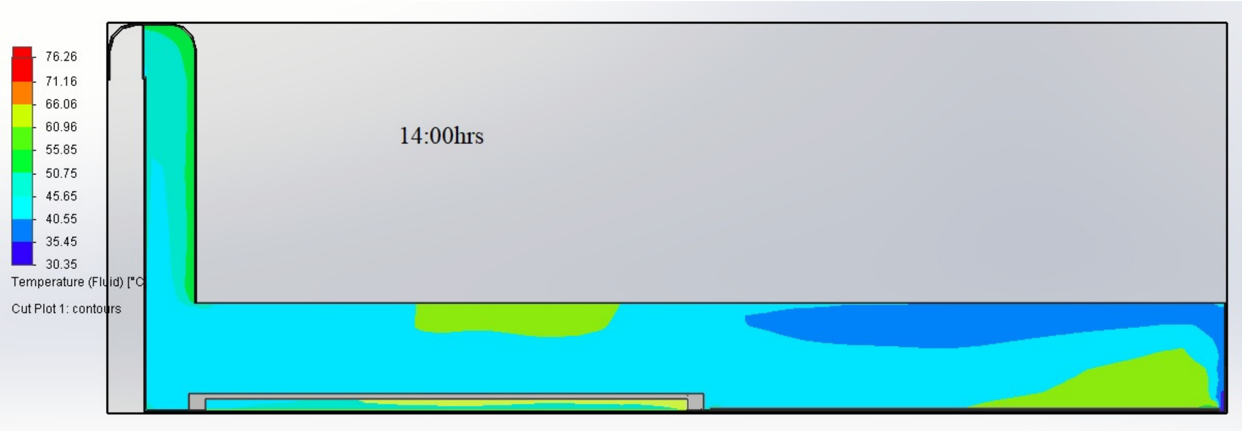

Figure 7. Temperature cut plot

3.1.2 Velocity

Figure 8 shows the velocity trajectories at 09:00, 12:00 and 15:00 hours. The air speed (velocity) picks up as it approaches the chimney exhaust vent. This pattern was anticipated because the flow cross-section reduces. The highest velocity is depicted at the inlet and outlet zones, which is caused by the apertures at both ends. It was also observed that the airflow velocity towards the drying unit produced the lowest velocity profile because the tray (wire mesh) and porous medium (banana slices) arrangement slightly obstructed the airflow stream across the drying unit, resulting in an average air velocity of 0.034 m/s.

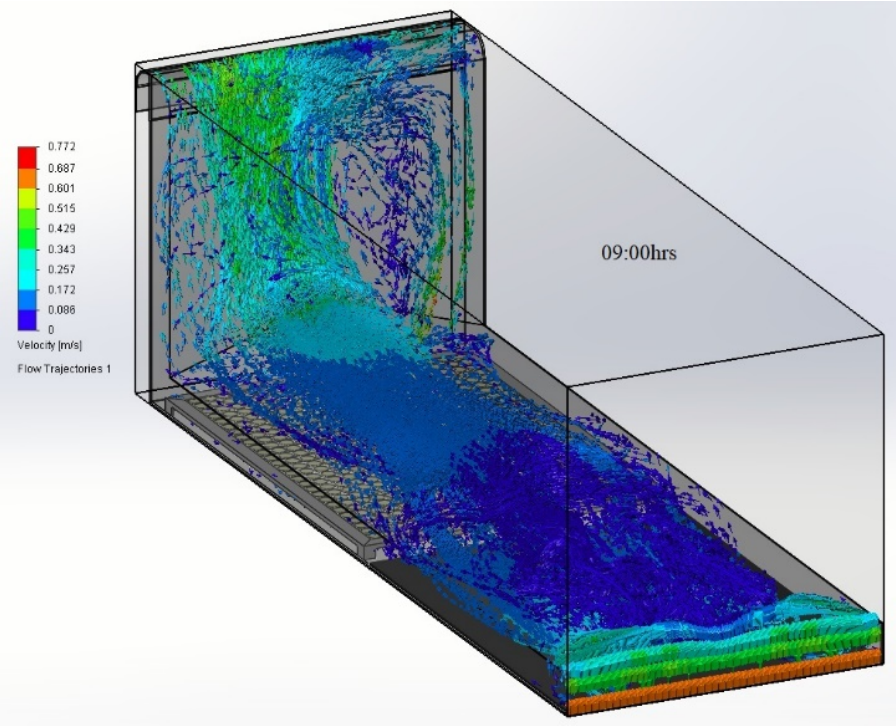
0.772
0.687
0.601
0.515
0.429
0.343
0.257
0.172
0.086
0
Velocity [m/s]
Flow Trajectories 1
09:00hrs

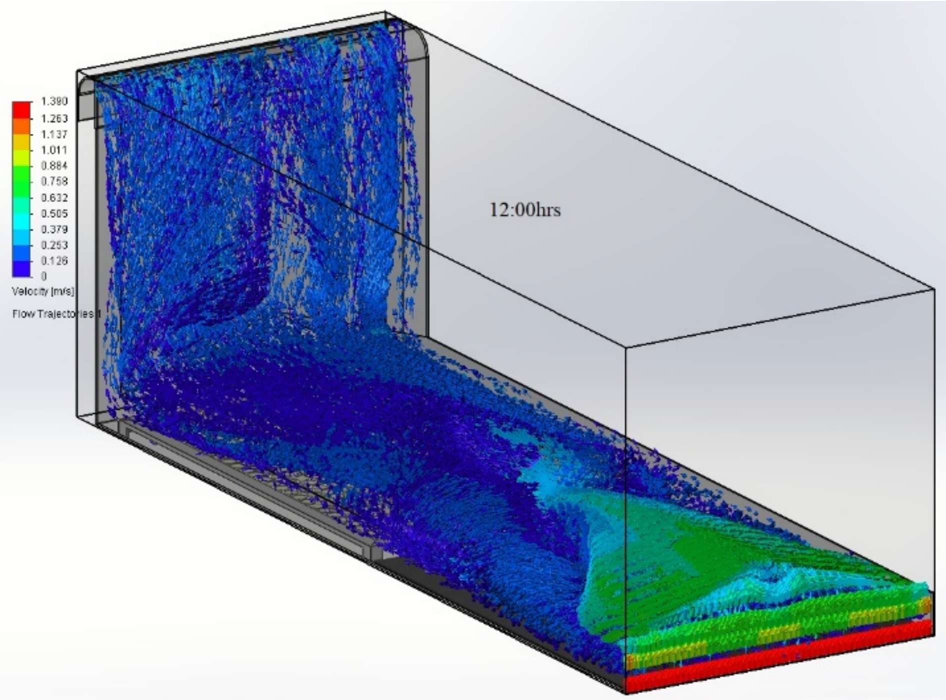
1.390
1.263
1.137
1.011
0.884
0.758
0.632
0.505
0.379
0.253
0.126
0
Velocity [m/s]
Flow Trajectories 1
12:00hrs

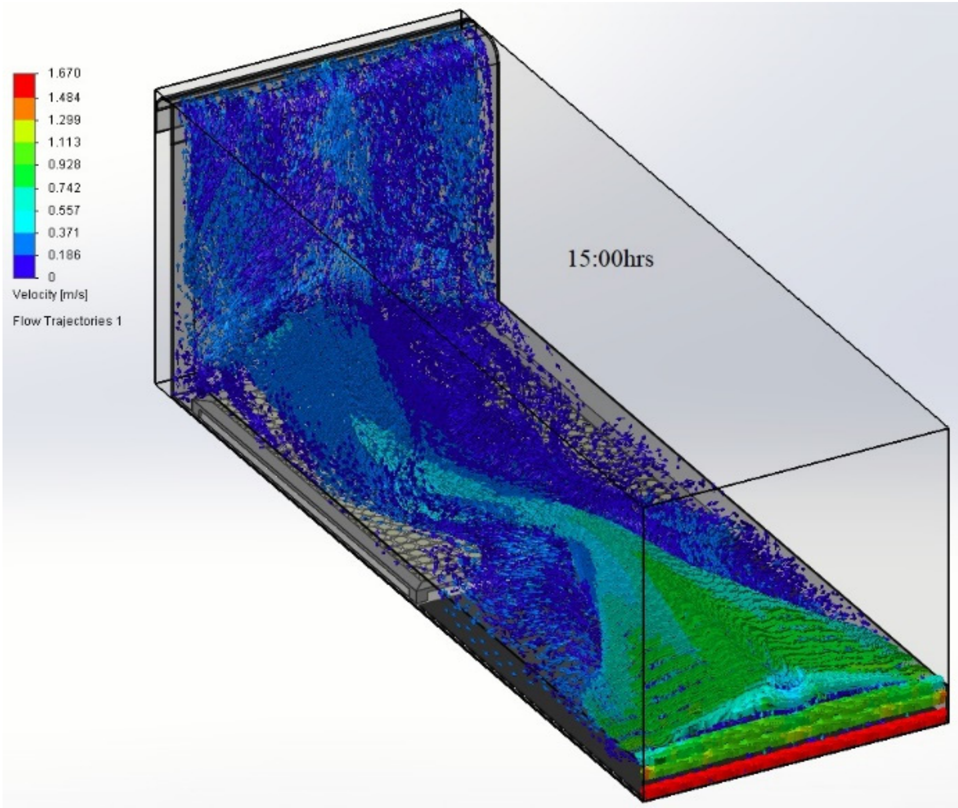

Figure 8. Velocity flow trajectories

Figure 9 shows velocity cut plot at 14:00 hours. The hottest air coming out of the collector forms a recirculation region before flowing to the drying unit. The hot air discharged by the collector rises because it is less dense and collides with each other when it reaches the polyethylene cover causing a disorderly flow field that forms a recirculation region. This flow pattern is in agreement with the cross-sectional temperature distribution depicted in Figures 6 and 7. The contours for the velocity shown in Figure 9 make it possible to appreciate the homogeneity of the temperature through the solar dryer. However, a decrease in the velocity in some parts of the dryer was observed. This was due to the loss in the velocity of the flux produced by the solids inside the chamber, which produced a uniform elevation of the heat.

Regarding the velocity, it was observed that the variation in the drying unit mesh favoured the velocity near the inlet. Hence, it was appreciated that the first pieces of fruit on the wire mesh, took most of the turbulence and backflows. However, when it reached the first bananas at a distance of 1.25 m from the inlet, its velocity dropped sharply to almost zero on the sides of the drying unit. This may have been due to the static resistance to its flow within the wire mesh and product. As the air left the drying unit, its velocity rose sharply but did not reach its initial value, stabilizing at an average of 0.055 m/s in the chimney. This could be attributed to the loss of some of its kinetic energy as it overcame the resistance to its flow through the wire mesh and product. Thus, the air velocity at the point on the wire mesh furthest from the air inlet, is less than that at the point closer. This agrees with the observations by Misha *et al*. (2013) that air velocity decreases as the distance from the inlet increases. Romuli et al. (2019) simulated airflow distribution and direction and estimated air mass flow in the inlet to be 0.75 kg/s in an inflatable solar dryer.

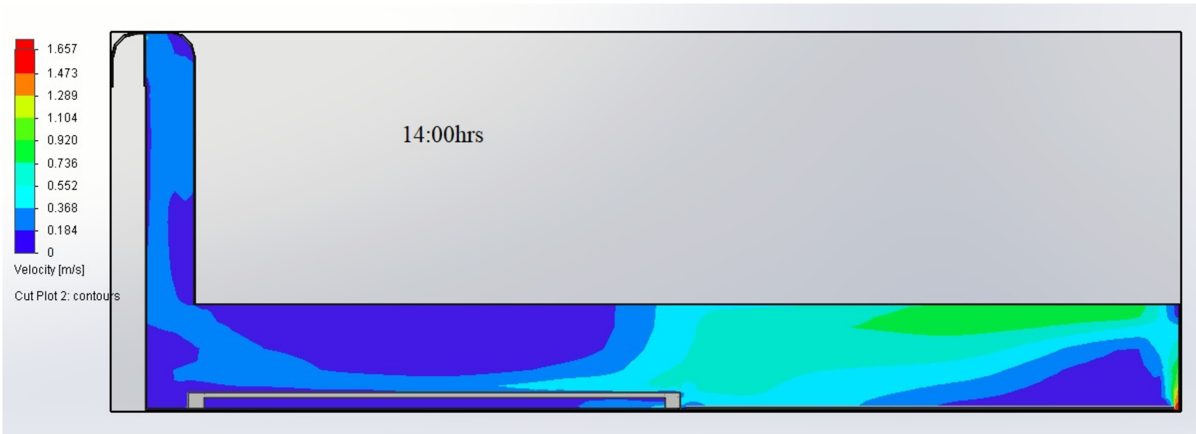

Figure 9. Velocity cut plot

It is also noted from Figure 9 that as the air flows from the drying chamber to the chimney it changes its direction of flow through a 90 degrees turn. According to Brooker et al. (1992), when air in a duct is forced to change it flow direction, both friction and dynamic losses are experienced, contributing to the total pressure losses. It is evident from Figure 9 that the airflow experiences some pressure losses as it moves from the drying chamber to the chimney, as seen by the change in its velocity. To reduce the losses, a curved joint is suggested to reduce the turbulence created as the air changes direction.

3.1.3 Chimney Buoyancy Effect

The chimney buoyancy effect depends on the rise in the temperature produced in the chimney. The simulation showed that the chimney's mean temperature increased by 18.73°C above ambient, thus producing the buoyancy effect. The drying unit air temperatures were higher than the chimney air temperatures despite the chimney receiving solar radiation to heat the air from the drying chamber, further. A major drawback of the bare flat plate type of chimney is its significant thermal losses, which may account for the cooling of the air observed in the chimney (Cherotich & Simate, 2016). The pressure drop that creates the airflow arising from the density difference between the ambient air and the chimney air, and the height of the chimney, can be seen in Figure 10. To cut down on the bare flat plate chimney's thermal losses, it is suggested, that its back and sides be insulated and a glazing added on its front side.

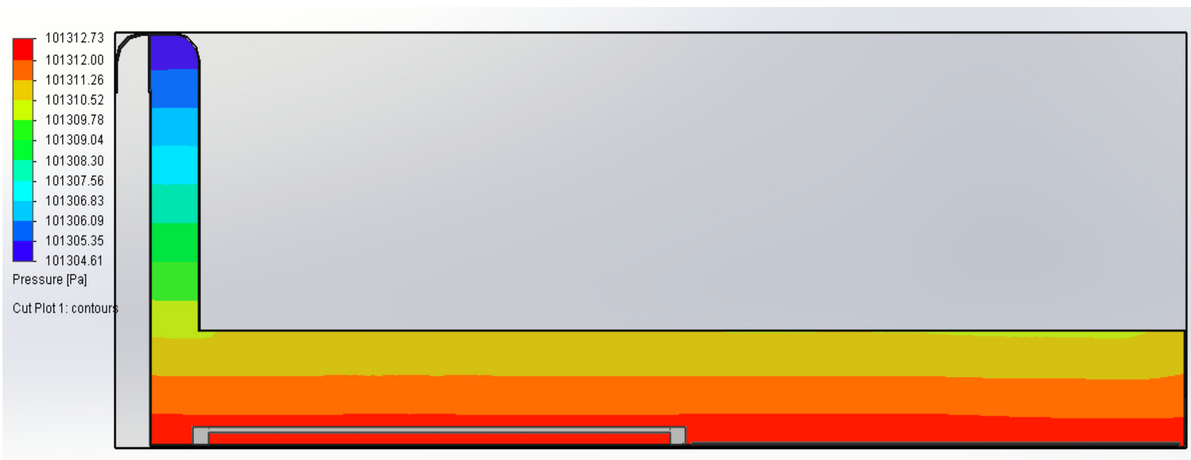

Figure 10. Pressure drop in the chimney

3.2 Comparison of Simulated and Experimental Results

3.2.1 Collector

The simulated and experimental results of the solar collector outlet air temperatures and the global solar radiation against time are shown in Figure 11. The simulated and experimental temperatures showed good agreement with the simulated results being higher by an average of 4.15 °C. The lower values of experimental results were probably caused by heat loss, which is affected by many factors of the surroundings, as the real conditions are not adiabatic. Consequently, the thermal efficiency of the collector from the simulation was found to be 37.63% which was greater than the efficiency of 33.09% obtained from the experiment.

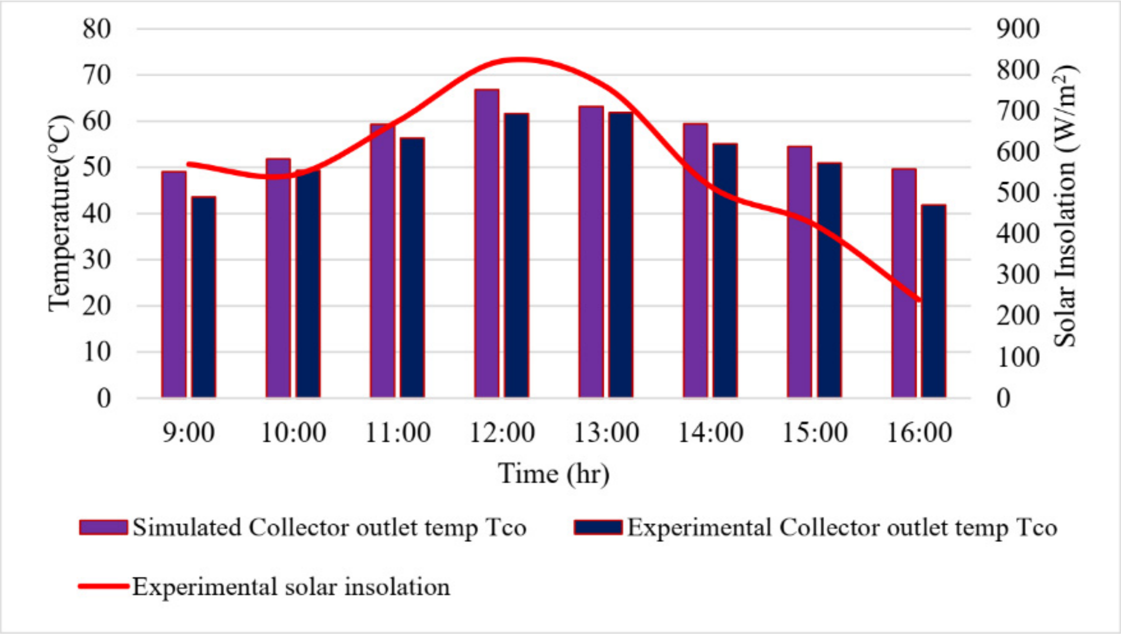

Figure 11. Average simulated and experimental temperatures at the collector outlet

3.2.2 Drying Unit

The comparison of simulated and experimental air temperatures in the drying chamber are shown in Figure 12. The results are in good agreement, with the average temperature difference of 3 °C. The simulated results were consistently higher than the experimental results because the simulation was set to be adiabatic while the experimental setup had some heat losses through some parts that did not have insulation. Both the simulated and experimental temperatures show a steady rise to a maximum of 73.96 and 70.65 °C respectively, followed by a steady decrease.

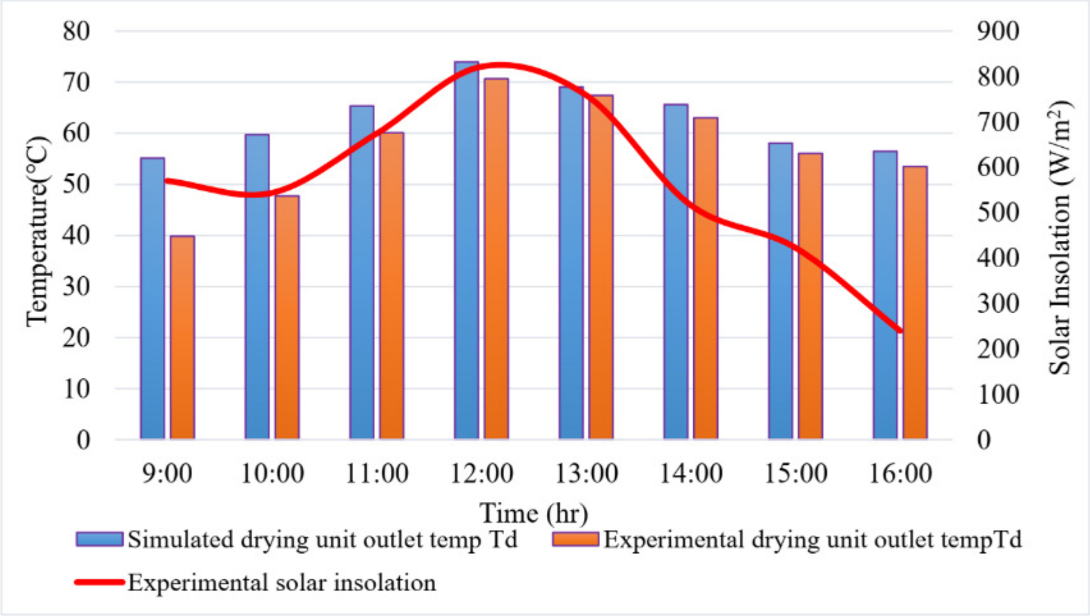

Figure 12. Average simulated and experimental temperatures in the drying unit

3.3 Mean Relative Deviation of Collector Temperature

The mean relative deviation (MRD) of collector temperature was obtained using Equation 1. A comparison between the numerical results and the experimental results shows a good agreement with a mean relative deviation of 5.1% which is acceptable as it does not exceed 10%. Other authors such as Tagne, et al., (2020) found an error of 4.53% which is almost equal to what was found in this study. From the low values of these errors, it can be inferred that the proposed model can predict the temperature profile inside the dryer satisfactorily. The relative error of 5.1 % is acceptable and can be explained by the fact that some real heat losses were not taken into consideration in the theoretical simulation.

4. Conclusion

This paper has set out to simulate, using CFD, the temperature and airflow distribution in a natural convection solar tunnel dryer. The following are noted:

(1) Although the chimney was receiving solar insolation through its absorber, the air in the chimney did not seem to have benefited from this heating, an indication that there was some loss of heat from the chimney. One way of reducing this heat loss from the chimney is to insulate its back and sides and add glazing on its front side.

(2) The hottest air coming out of the collector forms a recirculation region before flowing to the drying unit.

(3) The airflow experiences some pressure losses as it moves from the drying chamber to the chimney, as seen by the change in its velocity. To reduce the losses, a curved joint between the chimney and the drying chamber is suggested to reduce the turbulence created as the air changes direction.

(4) There existed a decrease in the velocity in some parts of the dryer. This was due to the loss in the velocity of the flux produced by the solids inside the drying chamber, which produced a uniform elevation of the heat.

(5) The simulation results were validated by comparing them with the results obtained from experiments. The results indicated a good agreement with a mean relative error of 5.1%.

It can be concluded that CFD is an efficient tool that can be used to predict the temperature and airflow distribution in natural convection solar tunnel dryers and has paved the way for further improvements in the design of these solar dryers.

Conflicts of Interest

The authors hereby declare that there are no conflicts of interest regarding the publication of this paper.

Acknowledgments

The authors wish to thank the Heads of the Department of Agricultural and Mechanical Engineering~~,~~ at the University of Zambia, Dr. V. Kaluba and Dr. V. Musonda together with their entire members of staff, technical and support staff for their generous input.

References

Al-Neama, M., & Farkas, I. (2016). Influencing of solar drying performance by chimney effect. *Hungarian Agricultural Engineering, 30*, 11-16. https://doi.org/10.17676/HAE.2016.30.11

Bala , B. K., & Wood, J. L. (1994). Simulation of the indirect natural convection solar drying of rough rice. *Solar Energy, 53*, 259-266. https://doi.org/10.1016/0038-092X(94)90632-7

Brooker, D., Bakker-Arkema, F., & Hall, C. (1992). *Drying and storage of grains and oilseeds*. Westport: The AVI Publishing Company.

Cherotich, S. (2016). *Experimental investigation and mathematical modelling of a natural convection solar tunnel fruit dryer*. Master of Engineering dissertation.

Cherotich, S., & Simate, I. N. (2016). Experimental Investigation and Mathematical Modelling of a Natural Convection Solar Tunnel Dryer. *International Journal of Scientific & Engineering Research, 7*(5), 597-603.

Jhersson, C.-R., Amaya, D., & Ramos, O. (2018). Food Dryer Design and Analysis of Velocity and Temperature Profiles. *International Journal of Applied Engineering Research, 13*(18), 13578-13583.

Kaushal, P., & Sharma, H. (2012). Concept of Computational Fluid Dynamics (CFD) and its Applications in Food Processing Equipment Design. *J Food Process Technol, 3*(138). https://doi.org/10.4172/2157-7110.1000138

Kumar, A., Sreenivaslu, G., P S Raghavendra, R., Kumar, A., & Pattanaik, A. (2019). Experimental Investigation on Performance of Solar Air Heaters With Thermal Storage. *International Journal of*

Renewable Energy and Its Commercialization, 5(1), 37-46. https://doi.org/10.37628/jrec.v5i1.770

Mathioulakis, E., Karathanos, V., & Belessiotis, V. (1998). Simulation of air movement in a dryer by computational fluid dynamics: application for the drying of fruits. *Journal of Food Engineering, 36*(2), 183-200. https://doi.org/10.1016/S0260-8774(98)00026-0

Michael, E. R. (2014). *Unit 03: Glazing - Greenhouse Management Online*. Retrieved May 23, 2022, from https://greenhouse.hosted.uark.edu/Unit03/Printer_Friendly.html

Misha, S., Mat, S., Ruslan, M. H., Sopian, K., & Salleh, E. (2013). The Prediction of Drying Uniformity in Tray Dryer System using CFD Simulation. *International Journal of Machine Learning and Computing, 3*(5), 419-423. https://doi.org/10.7763/IJMLC.2013.V3.352

Ni, H. (1997). *Multiphase Moisture Transport in Porous Media under Intensive Microwave Heating*. Ph.D Dissertation, . NY, USA: Cornell University, Ithaca.

Omolola, A. O., Jideani, A. I., & Kapila, P. F. (2015). Drying kinetics of banana (Musa spp.). *Interciencia, 40*(6), 374-380.

Roman, R. N., Lopez, O. A., Garcia, V., Pilatosky, F. I., & Ituna, Y. J. (2019). Computational fluid dynamics analysis of heat transfer in a greenhouse solar dryer "chapel-type" coupled to an air solar heating system. *Energy Sci Eng, 7*, 1123-1139. https://doi.org/10.1002/ese3.333

Romuli, S., Schock, S., Nagle, M., Chege, C. G., & Müller, J. (2019). Technical Performance of an Inflatable Solar Dryer for Drying Amaranth Leaves in Kenya. *Applied Science, 3*, 1-11. https://doi.org/10.3390/app9163431

Sangpradit, K. (2014). Study of the Solar Transmissivity of Plastic Cladding Materials and Influence of Dust and Dirt on Greenhouse Cultivations. *Energy Procedia, 56*, 566-573. https://doi.org/10.1016/j.egypro.2014.07.194

Simate, I. N. (2020). Air Flow Model for Mixed-Mode and Indirect-Mode Natural Convection Solar Drying of Maize. *Energy and Environment Research, 10*(2), 1-12. https://doi.org/10.5539/eer.v10n2p1

Simate, I. N., & Cherotich, S. (2017). Design and Testing of a Natural Convection Solar Tunnel Dryer for Mango. *Journal of Solar Energy,* 1-10. https://doi.org/10.1155/2017/4525141

SOLIDWORKS Corporation. (2010). *Engineering Design and Technology Series: An Introduction to Flow Analysis Applications with SolidWorks Flow Simulation, Instructor Guide*. Concord, Massachusetts USA: Dassault Systèmes - SolidWorks Corporation.

Tagne, M. S., Ndukwu, C. M., & Azese, N. M. (2020). Experimental Modelling of a Solar Dryer for Wood Fuel in Epinal (France). *Modelling, 1*, 39-52. https://doi.org/10.3390/modelling1010003

Tiris, C., Tiris, M., & Dincer, I. (1995). Investigation of the thermal efficiencies of a solar dryer. *Energy conversion and management, 36*, 205-212. https://doi.org/10.1016/0196-8904(94)00051-Z

Udomdejwatana, S. (1994). *Thermal properties of Musa suerier and Musa sapientum Linn, Master's Thesis*. Bangkok, Thailand: Chulalongkorn University.

Vintilă, M., Ghiaus, A. G., & Fătu, V. (2014). Prediction of Air Flow and Temperature Profiles Inside Convective Solar Dryer. *Bulletin of University of Agricultural Sciences and Veterinary Medicine Cluj-Napoca: Horticulture, 71*, 188-194. https://doi.org/10.15835/buasvmcn-fst:10868

Xia, B., & Sun, D.-W. (2002). Applications of computational fluid dynamics (CFD) in the food industry: a review. *Computers and Electronics in Agriculture, 34*, 5-24. https://doi.org/10.1016/S0168-1699(01)00177-6

Zoukit, A., El ferouali, H., Salhi, I., Doubabi, S., Abdenouri, N., & El kalali, T. (2019). Simulation, design and experimental performance evaluation of an innovative hybrid solar-gas dryer. *Energy, 189*, 116-279. https://doi.org/10.1016/j.energy.2019.116279

Copyrights

Copyright for this article is retained by the author(s), with first publication rights granted to the journal.

This is an open-access article distributed under the terms and conditions of the Creative Commons Attribution license (http://creativecommons.org/licenses/by/4.0/).